EXPERIMENTAL, COMPUTATIONAL, AND OBSERVATIONAL ANALYSIS OF PRIMORDIAL NUCLEOSYNTHESIS

Michael S. Smith

Physics Division, Oak Ridge National Laboratory

Abstract. We have made a comprehensive evaluation of the standard theory of primordial nucleosynthesis, by a) determining the nuclear reactions most important for light element production in the Big Bang; b) conducting a detailed study of the rates and uncertainties of these reactions; c) employing a Monte Carlo analysis to properly evaluate uncertainties in the computed elemental abundances arising from reaction rate uncertainties; and d) comparing the predicted abundances of d, ^{3}He, ^{4}He, and ^{7}Li to those inferred from observations. We find a consistent agreement for $2.86 \times 10^{-10} \leq \eta \leq 3.77 \times 10^{-10}$, where η is the baryon-to-photon ratio, thereby supporting the standard Big Bang nucleosynthesis (SBBN) theory. The corresponding constraint on the baryon density parameter is $0.01 \leq \Omega_b \leq 0.09$, where the primordial d+^{3}He (^{4}He) abundance sets the lower (upper) bound. We find that the new reaction rates increase the η upper bound from ^{7}Li by 45 %, and that inconsistencies in SBBN will arise if the primordial ^{4}He mass fraction is less than 0.237 or if the primordial ^{7}Li abundance is at the Pop I level. For slightly non-standard primordial nucleosynthesis models, comparisons to primordial abundances show that the number of neutrino families N_ν is limited to $N_\nu \leq 3.3$. Specifically, 3.5 neutrino families (3 Dirac ν's plus one Majorana ν) or more are ruled out at the 2-σ level. The dependence of the N_ν upper limit on the abundance limits has been parameterized.

1. INTRODUCTION

The current status of the standard primordial or Big Bang nucleosynthesis (SBBN) theory has been most recently reviewed by Krauss and Romanelli (1990) and by Walker *et al.* (1991). The work of Krauss and Romanelli is most notable for incorporating a Monte Carlo analysis into the abundance computations: their resulting 2-σ abundance curves allowed the full effect of reaction rate uncertainties on predicted abundances to be appreciated for the first time. Walker *et al.* concentrated primarily on a careful examination of the issues surrounding the extraction of limits on primordial abundances from current observations. Their analysis gave an upper bound on the baryon density of $\Omega_b \leq 0.10$. There are, however, a number of motivations for another examination of the SBBN model:

1. New Reaction Rates – It is important to utilize the latest tabulation of reaction rates by Caughlan and Fowler (1988) (hereafter CF88), and the even more recent measurements of the neutron lifetime and of the important d(d, n)^{3}He, d(d, p)t, t(α, γ)^{7}Li, ^{3}He(α, γ)^{7}Be, and ^{7}Li(p, α)^{4}He reactions.

2. Reexamination of Important Reaction Rates – We have done an extensive review of experimental data on reactions crucially important to Big Bang light-element production. Using all available data, we make a detailed determination of the reaction rates with uncertainties *appropriate for SBBN temperatures.*

3. Precise Abundance Uncertainties – Reaction rate uncertainties give the largest contribution to the SBBN predicted abundance uncertainties. We have utilized temperature-*dependent* rate uncertainties of the twelve most important reactions in a Monte Carlo analysis to transform reaction rate uncertainties into abundance uncertainties.

4. Correction of Computational errors – We correct for errors that arise from the linearization of the first-order differential equations used to time-evolve the abundances in the SBBN model. These errors, been neglected in previous SBBN studies, change the abundances for some elements by as much as 6 %.

5. New Inferred Primordial Abundances – Some recent theoretical work (Deliyannis and Pinsonneault 1993; Pinsonneault, Deliyannis, and Demarque 1992) have suggested that rotational effects can allow for essentially uniform ^{7}Li depletion in Pop II stars, making less certain the claim that the ^{7}Li abundances in these stars are primordial. This development calls into question previous upper limits on Ω_b obtained from the ^{7}Li abundance. There has also been recent work (Fuller, Boyd, and Kalen 1991) estimating a fairly low value for primordial ^{4}He, which has implications for the constraint on both Ω_b and N_ν.

6. A desire for caution – Previous SBBN studies have shown that the baryon density falls short of closing the Universe; however, we are less confident of the specific upper limits on the baryon density given by previous studies, and even less certain of a claimed inconsistency of the SBBN model with observations (Riley and Irvine 1991). Our goal is to find the most reasonable limits to Ω_b given cautious observational limits and a complete treatment of the reaction rates and numerical analysis.

7. A desire for completeness and comprehensiveness – We feel that the aspects of detailed analyses of nuclear reaction rates, numerical abundance predictions, and observational data should be brought

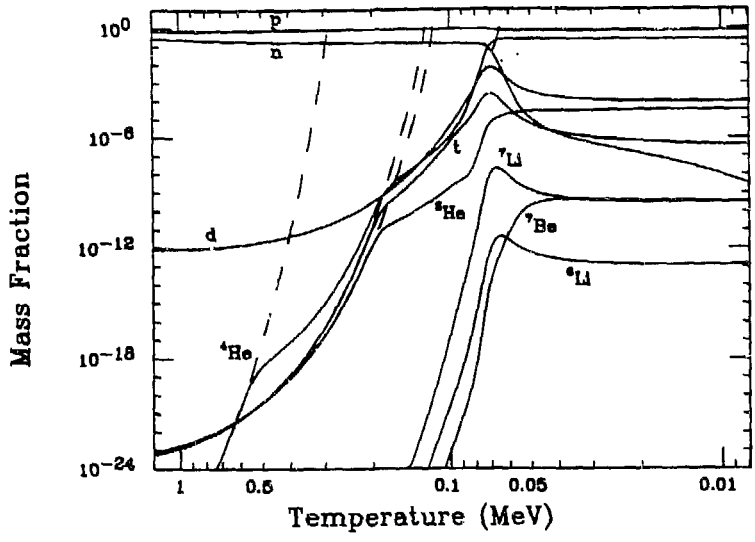

Figure 1. The evolution of light-element abundances with temperature for $\eta_{10} = 3.16$. The dashed curves are the NSE abundance curves of ^{4}He, t, ^{3}He, and d.

together in an up-to-date study to produce both a definitive picture of the current status of SBBN and a reliable constraint on the baryon density and the number of neutrino families.

These are the motivations for the comprehensive experimental, computational, and observational analysis of SBBN presented in Smith, Kawano, and Malaney (1993) (hereafter SKM), which emphasizes both experimental reaction rate measurements from the laboratory and the empirical abundance constraints from the observatory. We have used conservative 2-σ uncertainty levels on the computed abundances and conservative determinations of observational limits to put robust constraints on Ω_b and N_ν. Highlights of the new reaction rates, the most current observational limits, and our conclusions will be presented in these proceedings.

2. EVOLUTION OF ABUNDANCES AND PRIMARY REACTIONS

Standard Big Bang physics is reviewed in SKM and discussed in detail in, for example, Kolb and Turner (1990). A brief description of the temperature evolution of nuclide abundances will be presented here. We first note that the predominant process occuring in BBN is the assembly of (almost) all free neutrons (at the time of nucleosynthesis) into ^{4}He nuclei; only trace amounts of d and ^{3}He ($\sim 10^{-4}$) and ^{7}Li ($\sim 10^{-9}$) are formed relative to H. Nevertheless, it is the comparison of the precise predicted abundances of these trace nuclides (as well as ^{4}He) to observations which allow constraints to be placed on Ω_b and N_ν; the strength of the SBBN model will be evident from the agreement with abundances observations which span 9 orders of magnitude.

The temperature evolution of the neutron - proton ratio plays the crucial role in determining the two largest primordial abundances, H and ^{4}He. At high temperatures ($T \gg 0.8$ MeV), the weak interactions are fast enough to keep neutrons and protons in statistical equilibrium ($n/p = 1$). As the Universe cools, the neutron-proton mass difference $M_n - M_p = 1.293$ MeV ($\equiv Q$) reduces the number of neutrons relative to protons as $n/p = \exp(-Q/T)$. When the Universe has cooled to a temperature of about 0.8 MeV, the weak interaction rate - now comparable to the expansion rate - is no longer fast enough to keep neutrons and protons in equilibrium, and the n/p ratio is said to "freeze-out". The ratio actually continues to decrease slightly due to neutron decay, and at $T \approx 0.07$ MeV, most of the neutrons are processed into ^{4}He nuclei.

The amount of ^{4}He formed depends on the precise freeze-out temperature, arising from the competition between the expansion rate and the weak interaction rates. The expansion rate is parameterized by the number of light (mass $\ll 1$ MeV) relativistic degrees of freedom ($\propto N_\nu$): at any particular temperature, a larger N_ν corresponds to a larger expansion rate. Similarly, the weak interaction rates are parameterized by the neutron lifetime τ_n: a larger τ_n gives "weaker" weak interactions. The two rates are equal at the freeze-out temperature $T_* \propto N_\nu^{1/6} \tau_n^{1/4}$ (Steigman 1990), which results in $(n/p)_* \approx 1/6$.

An increase in N_ν therefore results a higher freeze-out temperature, a higher n/p ratio at freeze-out [$= \exp(-Q/T_*)$], and (since most neutrons get processed into ^{4}He) a larger ^{4}He abundance. A larger τ_n has the same effect of increasing the ^{4}He production. While the primordial ^{4}He mass fraction Y_p is directly proportional to N_ν and τ_n, it has only a logarithmic increase with increasing baryon density (parameterized by the baryon-to-photon ratio η, the baryon density in a volume element which expands with the universe; $\eta \sim 10^{-10}$). We note that N_ν is equal to 3 in the standard model, and that the uncertainty in τ_n accounts for ≈ 90 % of the uncertainty in the predicted ^{4}He abundance.

In order to determine the abundances of the trace isotopes as well as ^{4}He, we need to use the set of coupled first-order differential equations to time- (or temperature-) evolve the abundances, as first done in Wagoner (1969). Figure 1 shows the temperature evolution from the updated SBBN model (Kawano 1992) for 3 neutrino families and the value of $\eta = 10^{-9.5}$, or $\eta_{10} = 3.16$, where $\eta_{10} \equiv 10^{10}\eta$. By temperatures $T < 0.01$ MeV, nucleosynthesis has ended and the light element abundances have reached their predicted "primordial" values (which are dependent on the values of η and N_ν). From figure 1, we see that the evolution of the deuterium (d), tritium (t), ^{3}He, and ^{4}He nuclides is really a series of departures from nuclear statistical equilibrium (NSE). There are five temperatures at which these departures occur: 0.8 MeV, when neutrons and protons cease interacting with one another; 0.6 MeV, when ^{4}He leaves NSE; 0.2 MeV, when ^{3}He and t stop interacting with d; 0.08 MeV, when t and ^{3}He stop interacting with each other; and 0.07 MeV, when d finally falls out of equilibrium with n and p. This latter departure from NSE initiates the peak nucleosynthetic activity in the early universe, wherein most free neutrons are rapidly assimilated into ^{4}He. Trace amounts of the mass-7 nuclides are formed, and by $T \approx 0.04$ MeV nucleosynthesis ends and the light elements have reached their "primordial" abundances.

For temperatures above 0.6 MeV, the mass fractions are given by their NSE values. Were ^{4}He abundance to follow its NSE abundance curve (the dashed line in figure 1) to lower temperatures, it would dominate all the abundances by $T = 0.3$ MeV (note that this is significantly lower than the 28 MeV binding energy of ^{4}He). ^{4}He is, however, formed through ^{3}He and t and is therefore in NSE only through these two nuclides. The ^{3}He and t NSE abundances do not rise as fast as that for ^{4}He, so when the mass-3 and mass-4 NSE curves cross at $T \sim 0.6$ MeV, ^{4}He is forced to leave its NSE track and plod along with these mass-3 nuclides; this is a short-lived ^{3}He and t bottleneck. ^{4}He follows the mass-3 nuclides along their NSE curves until they too encounter a bottleneck at 0.2 MeV: the reactions d(n, γ)t and d(p, γ)^{3}He, which keep the mass-3 nuclides in equilibrium with d, slow down at this temperature. The abundances of ^{3}He, t, and ^{4}He are thus limited by the formation of deuterium (a minor "deuterium bottleneck"), and follow along the deuterium NSE curve. Note that ^{3}He, still in equilibrium with t via the ^{3}He(n, p)t reaction, has its abundance suppressed relative to that of t until $T = 0.08$ MeV when this reaction slows down. Finally, the deuterium abundance departs from its NSE track at about 0.07 MeV.

The relative contributions of individual nuclear reactions to the temperature evolution of the light-element abundances can be evaluated by examining the main channels of creation and destruction of each of the light elements d, t, ^{3}He, ^{4}He, ^{7}Li and ^{7}Be (this last nuclide decays to ^{7}Li after BBN ends). By ordering the creation and destruction rates (relative to the expansion rate) with respect to their value at the peak nucleosynthesis temperature, we find that 12 reactions are of primary importance in light element production: p(n, γ)d, d(p, γ)^{3}He, d(d, n)^{3}He, d(d, p)t, ^{3}He(n, p)t, t(d, n)^{4}He, ^{3}He(d, p)^{4}He, ^{3}He(α, γ)^{7}Be, t(α, γ)^{7}Li, ^{7}Be(n, p)^{7}Li, ^{7}Li(p, α)^{4}He, and the decay of the neutron. These 12 reactions form the basis of our experimental and computational analysis. We have thoroughly examined the experimental data on these reactions to produce best-fit reaction rates and reaction uncertainties (discussed in §3) which are used in a Monte Carlo analysis to determine the primordial abundances with uncertainties.

3. NUCLEAR REACTION RATES AND UNCERTAINTIES

3.1. Introduction

The procedure for obtaining thermonuclear reaction rates from laboratory cross section measurements is discussed, for example, in Fowler *et al.* (1967), Clayton (1983), and Rolfs and Rodney (1988). Rates for many astrophysically-important reactions are tabulated as analytic functions of temperature in the well-known compilations of Fowler *et al.* (1967), Fowler *et al.* (1975), Harris *et al.* (1983) (hereafter

known as FCZI, FCZII, and HFCZ, respectively), and CF88. Our analysis updates these compilations to include recent measurements of τ_n and of the d(d, n)^{3}He, d(d, p)t, ^{3}He(α, γ)^{7}Be, t(α, γ)^{7}Li, and ^{7}Li(p, α)^{4}He reactions. Our detailed reaction rate analysis additionally corrects a number of rates in CF88 that were formulated for temperatures of stellar nucleosynthesis – $T_9 \sim 10^{-3} - 10^{-1}$, where $T_9 = T(\mathrm{K})/10^9$ K – as opposed to those appropriate at Big Bang temperatures – $T_9 \sim 0.1$ to 1 ($T \sim$ 0.01 to 0.1 MeV).

In order to make robust light-element abundance predictions with our Monte Carlo analysis, we have quantitatively determined the uncertainties of the important SBBN reaction rates, some for the first time. An early estimate of rate uncertainties was made for a number of reactions in 1967 in FCZI, and ranged from 10 % to a factor of 2 for temperatures up to $T_9 = 10$. The primordial nucleosynthesis studies of Yang *et al.* (1984) and Walker *et al.* (1991) used a recent unpublished estimate of reaction rate uncertainties by Fowler and Caughlan, while the studies of Beaudet and Reeves (1984), Delbourgo-Salvador *et al.* (1985), and Riley and Irvine (1991) relied primarily on the uncertainties of a few recent measurements of individual cross sections. Krauss and Romanelli (1990) made the first quantitative study of the uncertainties of reaction rates utilizing *all* available data. However, they discussed only those reactions which had been recently remeasured, and they did not determine the uncertainties of the important ^{3}He(n, p)t and ^{3}He(d, p)^{4}He reactions. We expand on the work of Krauss and Romanelli to obtain appropriate reaction rates and uncertainties of the twelve reactions which are most important for Big Bang nucleosynthesis.

3.2. Reaction Rate Formalism

The formalism for the conversion of laboratory cross section measurements to thermonuclear reaction rates is thoroughly treated in SKM, where an emphasis is placed on the differences between primordial and stellar nucleosynthetic rates. Very briefly, this conversion involves a thermal average of the product of the cross section $\sigma(E)$ and relative velocity v over a Maxwell-Boltzman velocity distribution, and for charged particle reactions is often written as

$$N_a\langle\sigma \cdot v\rangle \propto T^{-3/2} \int_0^{+\infty} S(E) \exp(-(E_g/E)^{1/2} - E/kT)\, dE \ . \qquad (1)$$

where $N_a\langle\sigma \cdot v\rangle$ is the density-independent reaction rate, T is the temperature of the plasma, E is the center of mass energy, N_a is Avogadro's number, $S(E)$ is the Astrophysical S-factor (the cross section with the s-wave [$\ell = 0$] coulomb barrier penetrability and the geometric cross section $\pi\lambda^2 \propto E^{-1}$ divided out), and E_g is the Gamow energy. The slow energy variation of $S(E)$ makes it more easily extrapolated to low energies than $\sigma(E)$. The derivation of eq. (1), complete with numerical constants, is given in FCZI. The equivalent expression for neutron-induced reactions involves the function $R(E) = N_a \cdot \sigma \cdot v$ rather than the S-factor.

The integrand in eq. (1) is peaked at an effective energy $E_o = 122\ A^{1/3}\ (Z_1 Z_2)^{2/3}\ T_9^{\ 2/3}$ keV with a width $\Delta\ E_o = 237\ A^{1/6}\ (Z_1 Z_2)^{1/3}\ T_9^{5/6}$ keV, where A is the reduced mass and Z_i are the nuclear charges of the interacting species (Wagoner 1969). It is very important to accurately know the cross section over the appropriate *temperature-dependent* energy range $E_o \pm \Delta E_o$, since this range provides the dominant contribution to the thermal average in $N_a\langle\sigma \cdot v\rangle$ and since this range is quite different for stellar and primordial nucleosynthesis. For example, the effective energy range $E_o \pm \Delta E_o$ for the d(d, n)^{3}He reaction are 0.5 - 11 keV at $T_9 = 0.01$, 0 - 360 keV at $T_9 = 1.0$, and 0 - 1260 keV at $T_9 = 5.0$.

We analyzed the nonresonant contributions to the reaction rates by converting cross section data to S-factors, fitting to a smooth function of energy, and then analytically or numerically integrating eq. (1) to get the rate as a function of temperature. It is important to select the appropriate energy range for the S-factor fit: for example, a fit of the very low-energy d(d, n)^{3}He S-factor (for $E \leq 160$ keV, Krauss *et al.* 1987), suitable for the *stellar* reaction rate, is a factor of 2 (360) higher than the data a $E = 360$ (1260) keV, the top of the energy range $E_o + \Delta E_o$ at $T_9 = 1$ (5). The CF88 rate for this reaction based on the low-energy fit must therefore be modified for use in SBBN studies.

The analytical expressions for $S(E)$ and the derivations of the new rates of the 12 important SBBN reactions are thoroughly detailed in SKM. The analyses of five of the important reactions are given after the following section, and all the new rates are listed in table 1 along with their valid temperature ranges.

Table 1. Nuclear Reaction Rates*

	Reaction	Reference	Rate ($cm^3 s^{-1} mole^{-1}$)
1.	p(n, γ)d	SKM	4.742×10^4 $\times(1.-.850T_9^{1/2}+.490T_9-.0962T_9^{3/2}+8.47\times10^{-3}T_9^2-2.80\times10^{-4}T_9^{5/2})$
2.	d(p, γ)^{3}He	FCZII	$2.65\times10^3T_9^{-2/3}\exp(-3.720/T_9^{1/3})$ $\times(1.+.112T_9^{1/3}+1.99T_9^{2/3}+1.56T_9+.162T_9^{4/3}+.324T_9^{5/3})$
3.	d(d, n)^{3}He	SKM	$3.95\times10^8T_9^{-2/3}\exp(-4.259/T_9^{1/3})$ $\times(1.+.098T_9^{1/3}+.765T_9^{2/3}+.525T_9+9.61\times10^{-3}T_9^{4/3}+.0167T_9^{5/3})$
4.	d(d, p)t	FCZII	$4.17\times10^8T_9^{-2/3}\exp(-4.258/T_9^{1/3})$ $\times(1.+.098T_9^{1/3}+.518T_9^{2/3}+.355T_9-.010T_9^{4/3}-.0187T_9^{5/3})$
5.	^{3}He(n, p)t	SKM	$7.21\times10^8(1.-.508T_9^{1/2}+.228T_9)$
6.	t(d, n)^{4}He	SKM	$1.063\times10^{11}T_9^{-2/3}\exp[-4.559/T_9^{1/3}-(T_9/.0754)^2]$ $\times(1.+.092T_9^{1/3}-.375T_9^{2/3}-.242T_9+33.82T_9^{4/3}+55.42T_9^{5/3})$ $+8.047\times10^8T_9^{-2/3}\exp(-0.4857/T_9)$
7.	^{3}He(d, p)^{4}He	SKM	$5.021\times10^{10}T_9^{-2/3}\exp[-7.144/T_9^{1/3}-(T_9/.270)^2]$ $\times(1.+.058T_9^{1/3}+.603T_9^{2/3}+.245T_9+6.97T_9^{4/3}+7.19T_9^{5/3})$ $+5.212\times10^8/T_9^{1/2}\exp(-1.762/T_9)$
8.	^{3}He(α, γ)^{7}Be	SKM	$4.817\times10^6T_9^{-2/3}\exp(-14.964/T_9^{1/3})$ $\times(1.+.0325T_9^{1/3}-1.04\times10^{-3}T_9^{2/3}-2.37\times10^{-4}T_9-8.11\times10^{-5}T_9^{4/3}-4.69\times10^{-5}T_9^{5/3})$ $+5.938\times10^6T_{9a}^{5/6}T_9^{-3/2}\exp(-12.859/T_{9a}^{1/3})$ $T_{9a}=T_9/(1.+.1071T_9)$
9.	t(α, γ)^{7}Li	SKM	$3.032\times10^5T_9^{-2/3}\exp(-8.090/T_9^{1/3})$ $\times(1.+.0516T_9^{1/3}+.0229T_9^{2/3}+8.28\times10^{-3}T_9-3.28\times10^{-4}T_9^{4/3}-3.01\times10^{-4}T_9^{5/3})$ $+5.109\times10^5T_{9a}^{5/6}T_9^{-3/2}\exp(-8.068/T_{9a}^{1/3})$ $T_{9a}=T_9/(1.+.1378T_9)$
10.	^{7}Be(n, p)^{7}Li	SKM	$2.675\times10^9(1.-.560T_9^{1/2}+.179T_9-.0283T_9^{3/2}+2.21\times10^{-3}T_9^2-6.85\times10^{-5}T_9^{5/2})$ $+9.391\times10^8(T_{9a}/T_9)^{5/2}+4.467\times10^7T_9^{-3/2}\exp(-.07486/T_9)$ $T_{9a}=T_9/(1.+13.076T_9)$
11.	^{7}Li(p, α)^{4}He	SKM	$1.096\times10^9T_9^{-2/3}\exp(-8.472/T_9^{1/3})$ $-4.830\times10^8T_{9a}^{5/6}T_9^{-3/2}\exp(-8.472/T_{9a}^{1/3})$ $+1.06\times10^{10}T_9^{-3/2}\exp(-30.442/T_9)$ $+1.56\times10^5T_9^{-2/3}\exp[-8.472/T_9^{1/3}-(T_9/1.696)^2]$ $\times(1.+.049T_9^{1/3}-2.498T_9^{2/3}+.860T_9+3.518T_9^{4/3}+3.08T_9^{5/3})$ $+1.55\times10^6T_9^{-3/2}\exp(-4.478/T_9)$ $T_{9a}=T_9/(1.+.759T_9)$
12.	Neutron Decay	SKM	$\tau_n=888.54$ seconds

* Valid T_9 Ranges: 0.01 - 2 [Reactions 3, 4, 5, 6, 7, 8, 9, 11], 0.01 - 6 [2, 5], 0.01 - 20 [10], & 0.01 - 100 [1].

3.3. Reaction Rate Uncertainties

The contributions to the total reaction rate uncertainty include the statistical and systematic uncertainties of the laboratory cross section measurements, the uncertainty in the parameters of a smooth fit to the S-factor as a function of energy, and the uncertainty in an analytic approximation to the thermal average of $\sigma \cdot v$. Statistical uncertainties range from 2 to 20 %, with more recent measurements giving (in general) greater precision; and fitting uncertainties are typically less than 5 %. It is the systematic uncertainties, as evidenced by the scatter of the cross section values from different experiments, that typically provide the dominant contribution to the total uncertainty. For some reactions, different measurements barely overlap at the 2-σ level; in these cases, a reasonable consideration of *all* of the

Table 2. Nuclear Reaction Rate Uncertainties

Reaction	1-σ Uncertainty (%)
1. p(n, γ)d	7
2. d(p, γ)^{3}He	10
3. d(d, n)^{3}He	10
4. d(d, p)t	10
5. ^{3}He(n, p)t	10
6. t(d, n)^{4}He	8
7. ^{3}He(d, p)^{4}He	8
8. ^{3}He(α, γ)^{7}Be	$T_9 \leq 10$: $(27. - 15.T_{9b}^{1/2} + 4.0T_{9b} - .25T_{9b}^{3/2} - .02T_{9b}^2)$, $T_{9b} = T_9 + .783$
	$T_9 > 10$: 9.7
9. t(α, γ)^{7}Li	$T_9 \leq 10$: $(29. - 5.9T_{9b}^{1/2} - 7.2T_{9b} + 4.0T_{9b}^{3/2} - .56T_{9b}^2)$, $T_{9b} = T_9 + .0419$
	$T_9 > 10$: 8.1
10. ^{7}Be(n, p)^{7}Li	9
11. ^{7}Li(p, α)^{4}He	8
12. Neutron Decay	0.42

data forces the total uncertainty to be significantly larger than that of the most precise measurement in the dataset. In effort to obtain robust abundance predictions, we have chosen conservative S-factor uncertainties such that $\sim$ 95 % of the data are included at the 2-σ level.

$S(E)$ is often written with a leading term $S(0)$, and the S-factor uncertainty is often expressed as a fractional uncertainty in $S(0)$. The reaction rate is then proportional to $S(0)$, and an energy-*independent* fractional uncertainty in the S-factor will result in the same temperature-*independent* fractional uncertainty in the reaction rate. Note that the uncertainty appropriate for rates at Big Bang temperatures does *not* include the uncertainty in the extrapolation of $S(E)$ to zero energy, as is appropriate for stellar nucleosynthesis rates. With this in mind, we have assigned an energy-independent uncertainty characteristic of the S-factor uncertainty over $E_o \pm \Delta E_o$ to all but two of the reactions under consideration.

The t(α, γ)^{7}Li and ^{3}He(α, γ)^{7}Be reactions do, however, require an energy-*dependent* uncertainty in $S(E)$ because of large discrepancies in different measurements of $S(E)$ at low energies. The energy-*dependent* uncertainties in $S(E)$ result in temperature-*dependent* reaction rate uncertainties after thermal averaging. If a symmetric 2-σ uncertainty in $S(E)$ is given by

$$S(E)_{\pm 2\sigma} \;=\; S(E)\;(\;1\;\pm\;f(E)\;)\;, \tag{2}$$

for some function $f(E)$, the corresponding thermally averaged reaction rates $N_a\langle\sigma\cdot v\rangle_{\pm 2\sigma}$ are not symmetric about $N_a\langle\sigma\cdot v\rangle$. In order to ease the computational requirements in the Monte Carlo procedure described in § 4, the S-factor uncertainties were iteratively adjusted to produce the symmetric reaction rate uncertainty

$$N_a\langle\sigma\cdot v\rangle_{\pm 2\sigma} \;=\; N_a\langle\sigma\cdot v\rangle\;(\;1\;\pm\;g(T)\;)\;, \tag{3}$$

where the function $g(T)$ is given as a power series in $T^{n/2}$.

The uncertainties of the twelve important SBBN reactions are summarized in table 2, and five of the reactions are discussed in detail in the next sections.

3.4. The p(n, γ)d Reaction

This is the reaction which initiates primordial nucleosynthesis. The analytic expression for this reaction rate has not changed since the FCZI compilation, which used theoretical calculations of deuteron photodissociation (Bethe and Morrison 1956, Evans 1955) normalized to the thermal neutron capture cross section measurement of Hughes and Schwartz (1958) ($\sigma_{th} = 0.332 \pm 0.002$ b). The most recent p(n, γ)d evaluation is from Hale *et al.* (1991), who relied on the latest thermal neutron capture measurement of 0.3326 $\pm$ 0.006 b (Mughabghab *et al.* 1983), higher energy data (18 - 36 MeV) from Bosman *et al.* (1979), and deuteron photodissociation and neutron capture data from previous recent evaluations.

For energies $E > 0.1$ MeV, there is a substantial discrepancy between the rate derived from the Hale *et al.* data evaluation and the FCZI rate, as evident from the plot of $R(E)$ in figure 2. We have therefore made a new fit of $R(E)$ up to 25 MeV to within 5 % of Hale *et al.*; $R(E)$ was taken as a constant for

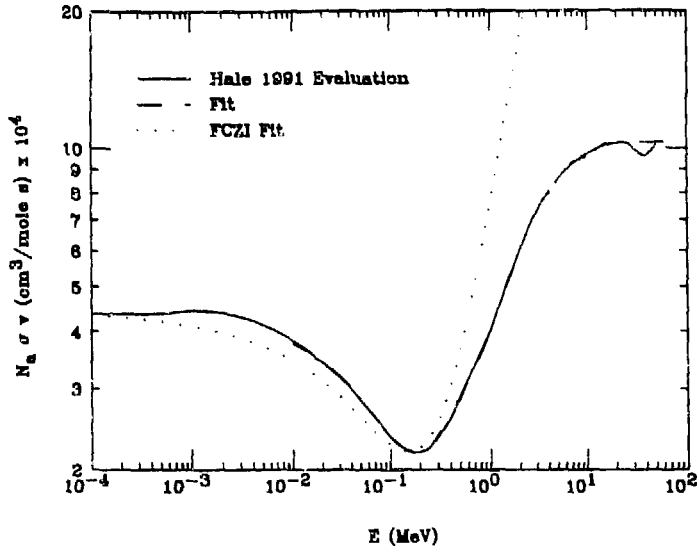

Figure 2. The p(n, γ)d data evaluation of Hale *et al.* 1991 and polynomial fits to $R(E)$ from the present work and from FCZI/CF88.

higher energies. This new fit is shown as the dashed line in figure 2. The thermal average was found by numerical integration from 0.1 keV to 100 MeV at temperatures $0.01 < T_9 < 100.0$ and was fit to the rate given in table 1 to within 2 %. The uncertainty of the recommended cross section values, quoted from Hale *et al.*, is 0.2 %; previous compilations have higher uncertainties (Horsley 1966, 2 %; Howerton 1959, 5 %). We will assume a conservative 5 % uncertainty in the evaluation, which, when combined in quadrature with the 5 % fit of $R(E)$ and the 2 % fit of the numerical integration gives a total 1-σ uncertainty of 7 %.

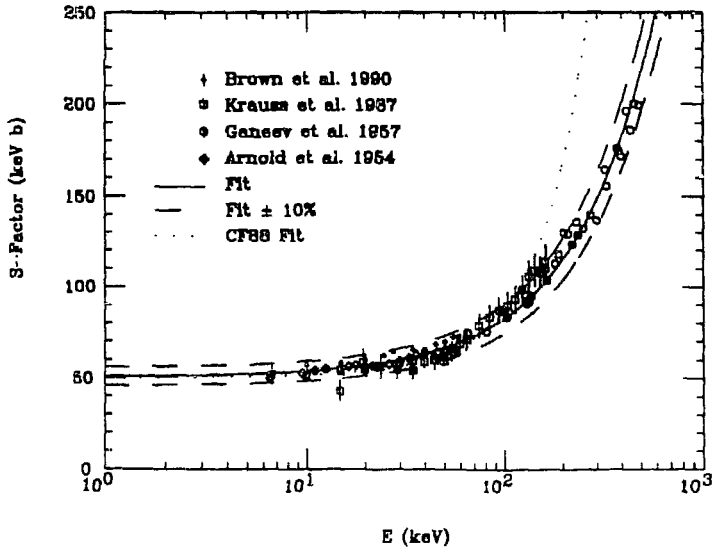

Figure 3. d(d, n)^{3}He S-factor data and polynomial fits from FCZII and CF88. The dashed curves show the 1-σ uncertainty of 10 %.

3.5. The d(d, n)^{3}He and d(d, p)t Reactions

The d(d, n)^{3}He reaction, most important for ^{3}He production, has been recently measured by Krauss *et al.* (1987) for $E \leq 160$ keV and very precisely by Brown *et al.* (1990) for $E \leq 60$ keV. Previous measurements include Arnold *et al.* (1954) ($E \leq 55$ keV) and Ganeev *et al.* (1967) ($E \leq 1$ MeV). The polynomial S-factor fit of Krauss *et al.*, used for the rate in the CF88 compilation, increases more

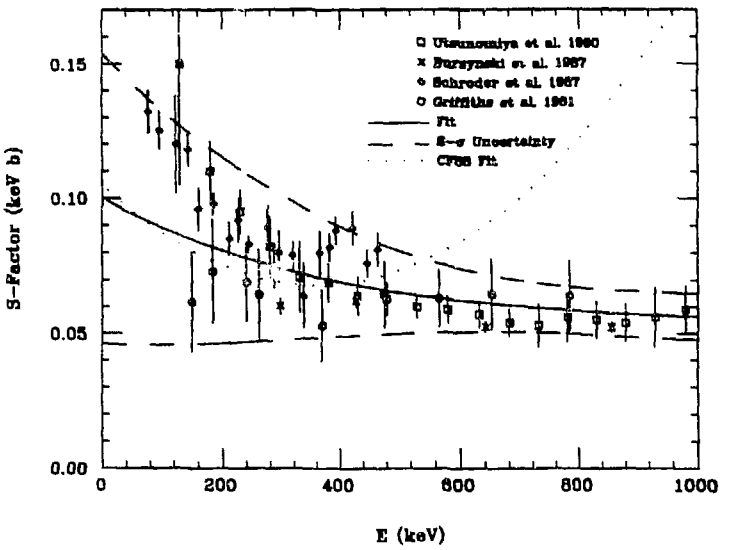

Figure 4. t(α, γ)^{7}Li S-factor data and fits from the present work and from CF88. The dashed curves show the energy-dependent 2-σ S-factor uncertainty.

rapidly with energy than the data for $E > 150$ keV, as shown in figure 3. The polynomial S-factor fit used in FCZII is a good fit to the data for $E < 300$ keV; however, their fit leads to negative reaction rate values for $T_9 > 20$ after thermally averaging $S(E)$. Therefore, we have made a new polynomial S-factor fit to the four measurements listed above, and thermally averaged $S(E)$ analytically to get the new d(d, n)^{3}He reaction rate valid for $T_9 < 100$. Since the data of Brown *et al.*, quoted to a precision of 1 - 2 %, differ by up to 10 % from the measurements of Krauss *et al.* (with an uncertainty of 6 - 8 %), the total uncertainty must reflect the scatter of these two measurements. A conservative 1-σ S-factor uncertainty of 10 % includes all of the data up to 500 keV and is shown in figure 3; this 10 % uncertainty is appropriate for the d(d, n)^{3}He reaction rate.

As with the d(d, n)^{3}He reaction, the d(d, p)t S-factor fit used in CF88 (from Krauss *et al.*) increases more rapidly with energy than the data for $E > 150$ keV, whereas the S-factor fit used by FCZII is a good fit to all of the data. The d(d, p) reaction rate derived analytically from this S-factor is valid for $T_9 < 10$, the temperatures where tritium is produced via d(d, p)t. A conservative 1-σ uncertainty of 10 % is necessary to include the scatter of all the S-factor data; this 10 % uncertainty is also appropriate for the d(d, p)t reaction rate uncertainty. A precision measurement of d(d, n)^{3}He and d(d, p)t at energies up to 1 MeV would substantially reduce the dependence of these rates on the measurement of Ganeev *et al.* (1957).

3.6. The t(α, γ)^{7}Li Reaction

This reaction dominates ^{7}Li production at low baryon densities (low η values) during SBBN. Because of the difficulty of fabricating tritium targets, there have been only three capture γ-ray measurements of t(α, γ)^{7}Li at energies ranging from 0.08 to 1.8 MeV: Schroder *et al.* (1987), Burzynski *et al.* (1987), and Griffiths *et al.* (1981). While the measurements of Griffiths *et al.* and Burzynski *et al.* are consistent with an energy-independent S-factor of 0.064 keV b for $E > 150$ keV, the measurement of Schroder *et al.* shows a substantial rise in $S(E)$ with decreasing energy down to 80 keV: their extrapolation to zero energy is $S(0) = 0.14 \pm 0.02$ keV b, more than a factor of two larger than previous measurements. A preliminary result of a new capture γ-ray experiment by Brune *et al.* (1991) confirms a rising S-factor with decreasing energy, although their S-factor rises less steeply than that of Schroder *et al.* Finally, a measurement has been made by Utsunomiya *et al.* (1990) employing the Coulomb breakup of ^{7}Li induced by the ^{208}Pb(^{7}Li, α t)^{208}Pb reaction at 6 and 9 MeV/u. Their data, normalized to Griffiths *et al.* at $E = 500$ keV, exhibit the most rapid rise in $S(E)$ with decreasing energy of all the experiments. The data from the four published experiments are plotted in figure 4.

There are potential difficulties, however, with the interpretation of the results of Utsunomiya *et al.* First, there has been some question of the theory relating Coulomb breakup data to radiative-capture rates as originally proposed by Baur *et al.* (1986), especially the requirement that there be no interference between the Coulomb and nuclear contributions to the cross sections. This difficulty is much worse

for non-resonant breakup reactions, such as t(α, γ)^{7}Li, than for resonant breakup reactions. Measurements of Coulomb-breakup cross sections by Hill *et al.* (1991) indicate a smaller projectile-charge (Z) dependence than predicted by calculation (a factor of two at low Z), suggesting that artificially large capture cross sections may be predicted from this technique. Measurements by Mason *et al.* (1992) of ^{12}C,^{197}Au(^{7}Li, α t) at 8 MeV/u confirm that nuclear cross section effects, as well as target-proximity effects, are present in the breakup cross sections.

There is also a potential problem with the experiment of Schroder *et al.*: the branching ratio for t + ^{4}He capture into the ^{7}Li ground state ($J^\pi = 3/2^-$) to t + ^{4}He capture into the $E_x = 0.478$ MeV excited state ($J^\pi = 1/2^-$) differs from the values measured by Griffiths *et al.* and Burzynski *et al.*, as well as from the calculations of Altmeyer *et al.* (1988) and Kajino *et al.* (1989). The effect of this problem on the S-factor energy dependence (of primary importance in this study) is, however, uncertain.

Finally, a recent measurement of the t(p, γ)^{4}He cross section by Feldman *et al.* (1990) calls into question value from Perry and Bame (1957) used by Schroder *et al.* and Griffiths *et al.* to determine tritium target thicknesses. This has ramifications for the overall normalization of $S(E)$ but not for the S-factor energy dependence.

Until additional measurements of the S-factor energy dependence are made, the results of the Utsunomiya *et al.*, Schroder *et al.*, Burzynski *et al.*, and Griffiths *et al.* will be used to determine a new t(α, γ)^{7}Li reaction rate. The analytic expression for this rate in the FCZI and FCZII compilations was obtained from a constant S-factor equal to 0.064 keV b from Griffiths *et al.* Langanke (1986) used a microscopic potential model for the S-factor which indicates a substantial rise in $S(E)$ with decreasing energy, with an extrapolated value $S(0) = 0.105$ keV b. RGM calculations made by Kajino and Arima (1984), Mertelmeier and Hofmann (1986), Kajino (1986), and Kajino *et al.* (1987) also predict a rise in $S(E)$ with decreasing energy. Kajino *et al.* derive a polynomial times a decreasing exponential form for the S-factor with an extrapolated value of $S(0) = 0.100 \pm 0.025$ keV b.

Langanke made a polynomial fit to his microscopic potential model S-factor *at low energies* to obtain the reaction rate used in CF88. As shown by the dotted curve in figure 4, however, this polynomial fit is not appropriate for $E \gtrsim 400$ keV. Since figure 1 shows that processing of ^{7}Li begins at temperatures of $T \approx 0.1$ MeV ($T_9 \approx 1$), where the effective energy range $E_o \pm \Delta E_o$ is from 0 to 550 keV, the low-energy S-factor fit used for the CF88 rate should not be used for SBBN studies. We have therefore made a new least-squares fit of the S-factor data up to $E = 2$ MeV, using a polynomial plus a decreasing exponential form (from RGM calculations of Kajino, Toki, and Austin 1987) and fixing the value of $S(0)$ to be 0.100 keV b; the result is

$$S(E) = 0.100 \left(1 + 3.774 \cdot 10^{-5} E \right) + 0.0522 \left(\exp(-2.411 \cdot 10^{-3} E) - 1 \right) \text{ keV b} \qquad (4)$$

for energies E in keV. Above 2.0 MeV, $S(E)$ is taken to be constant. This S-factor, shown as the solid curve in figure 4, was thermally averaged by numerically integrating eq. (1) from 1 keV to 100 MeV at temperatures $0.01 < T_9 < 100.0$, and was fit within 3 % to the rate given in table 1. The new rate is substantially smaller than the previous CF88 rate; the discrepancy is a factor of 2 at $T_9 = 3$. This results in significantly less production of ^{7}Li via t(α, γ)^{7}Li than previously estimated.

This S-factor requires an energy-*dependent* uncertainty due to the large spread in measured values at low energies. The function $g(T)$ for the symmetric 2-σ reaction rate uncertainty (eq. 3) is given by

$$g(T) = 0.572 - 0.118\, T_{9b}^{1/2} - 0.145\, T_{9b} + 7.97 \cdot 10^{-2}\, T_{9b}^{3/2} - 1.11 \cdot 10^{-2}\, T_{9b}^{2} \qquad (5)$$

for $T_9 < 10$, where $T_{9b} = T_9 + 0.0419$, and $g(T) = 0.161$ for $T_9 > 10$. The S-factor uncertainty is plotted in figure 4 as the dashed curves. The 1-σ reaction rate uncertainties are 26 % at $T_9 = 0.01$, 19 % at $T_9 = 1$, and 8 % at $T_9 > 10$.

3.7. Neutron Decay

The lifetime τ_n of the free neutron decay characterizes the strength of the neutron-proton weak interaction, and the amount of ^{4}He produced during primordial nucleosynthesis is directly proportional to τ_n. Recent lifetime measurements have produced lower values of the neutron lifetime, implying less primordial ^{4}He production. The experiments have traditionally utilized an in-beam method, where decay products (electrons or protons) are counted near a slow neutron beam (see the reviews of Dubbers 1991, Freedman 1990, and Byrne 1982); a newer set of experiments have utilized neutron storage devices (traps), in which the number of neutrons surviving in a trap are counted as a function of time. Storage

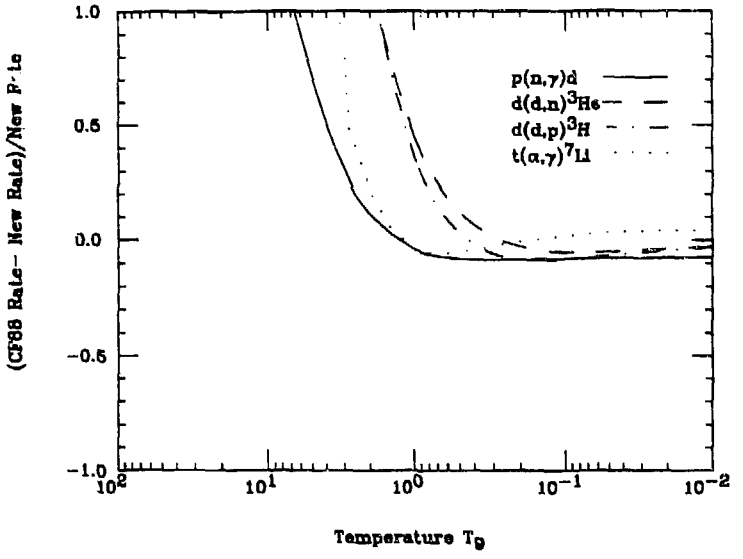

Figure 5. The fractional reaction rate difference from CF88 vs. temperature for the p(n, γ)d, d(d, n)^{3}He, d(d, p)t, and t(α, γ)^{7}Li reactions.

methods have exploited, for example, the neutron magnetic moment and the reflection properties of ultracold walls. Significant reductions in systematic uncertainties of trap methods have yielded the most precise lifetime measurements to date (e.g. Mampe *et al.* 1989). A complete list of the measurements, including very early and preliminary measurements, is given in SKM. In light of the recent use of a pulsed neutron beam (Last *et al.* 1988) and the significant experimental advances in trap techniques since 1986, we have followed Freedman and used the weighted mean of all lifetime measurements since 1986 (888.5 $\pm$ 3.8 s, 2-σ) in our analysis. In our conservative approach, we have doubled this purely statistical uncertainty in our Monte Carlo routine to account for systematic uncertainties in the measurements; this is discussed in §6. We have not utilized any estimates of τ_n based on angular correlation measurements and weak coupling constant values, and we did not include the value from Spivak (1988) reanalysis of the Bondarenko *et al.* (1978) measurement. The average of all (including pre-1986) measurements is 889.8 $\pm$ 3.6 s (2-σ), agreeing within error with the mean of the recent measurements.

3.8. Comparison of New and Previous Rates

In order to compare the rates used in our reaction network and Monte Carlo analysis with the CF88 rates, we have plotted the fractional rate difference (CF88 rate - present rate / present rate) as a function of temperature in figure 5 for the four reactions differing the most from CF88: p(n, γ)d, d(d, n)^{3}He, d(d, p)t, and t(α, γ)^{7}Li. These new rates are more than a factor of two lower than the CF88 rates for temperatures $T_9 \gtrsim$ 7, 2, 2, and 3, respectively. Over the important temperature range T_9 = 0.1 to 10, the d(p, γ)^{3}He, t(d, n)^{4}He, ^{3}He(d, p)^{4}He, ^{3}He(α, γ)^{7}Be, ^{7}Li(p, α)^{4}He, and ^{7}Be(n, p)^{7}Li reactions differ by less than 20 % from the corresponding CF88 rate. The effect of these new rates on the predicted abundances is discussed in the following section.

4. NUMERICAL ANALYSIS AND RESULTS

Our Monte Carlo analysis, which determines the overall effect of the reaction rate uncertainties on the predicted light-element abundances, involves representing each of the 12 important rates by a gaussian distribution centered on a mean rate value (table 1) with a width given by the rate uncertainty (table 2). In contrast with the analysis of Krauss and Romanelli (1990), we used temperature-dependent rate uncertainties where necessary. For a particular computer run at a particular value of η and N_ν, we generated a random number for each of the 12 reactions to determine new reaction rates by generating a displacement from the mean rate. We incorporated these features into the latest adaptation of Wagoner's code (Kawano 1992), along with the 12 new reaction rates discussed in §3 and the (other unchanged) rates from CF88. We then computed the light-element abundances, compensating for computational

Table 3. Effects of New Reaction Rates*

Reaction	d	^{3}He	^{4}He	^{7}Li
p(n, γ)d	-1.59	1.37	0.03	11.05
d(p, γ)^{3}He	5.62	-5.74	0.00	-9.24
d(d, n)^{3}He	8.67	-0.41	-0.17	-12.04
d(d, p)t	2.42	1.72	-0.11	-2.04
^{3}He(n, p)t	-0.79	4.42	0.00	7.59
t(d, n)^{4}He	0.01	0.03	0.00	-0.12
^{3}He(d, p)^{4}He	-0.40	-5.89	0.00	-5.35
^{3}He(α, γ)^{7}Be	0.00	0.00	0.00	-7.59
t(α, γ)^{7}Li	0.00	0.00	0.00	0.04
^{7}Be(n, p)^{7}Li	0.00	0.00	0.00	2.02
^{7}Li(p, α)^{4}He	0.00	0.00	0.00	0.00
All Reactions	15.06	-5.36	-0.27	-18.22

*Percentage change from abundances with CF88 rates at $\eta_{10} = 6.0$

errors associated with the linearizations in the Runge-Kutta method and in the abundance-changing differential equation; these corrections can be as great as 6 % (Kawano 1992). We also corrected the ^{4}He mass fraction by subtracting 0.0025 to account for the analytic approximations used for the p $\leftrightarrow$ n rates (Dicus *et al.* 1982).

For each value of the baryon-to-photon ratio η, we did 1000 such runs of the computer program and represented the results by a mean value and a 2-σ standard deviation of the abundances of D, ^{3}He, ^{4}He, and ^{7}Li. We covered the range in η_{10} from 1 to 10 with 15 values, using a higher density of points around the ^{7}Li "dip" near $\eta_{10} = 3$. We first restricted our calculations to the case of 3 relativistic neutrino families (the standard model), and then extended to cosmologies with N_ν ranging from 2.5 to 5.0; the results for nonstandard models will be discussed in §7.

We have plotted the computed abundances for ^{4}He (mass fraction), (d+^{3}He)/H, and ^{7}Li/H against η in figure 6 for the standard model ($N_\nu = 3$). The continuous curves give the mean computed values for the elemental abundances, and the dashed lines give the 2-σ abundance curves. The boxes and other lines show the abundance constraints from observations listed in table 4 and discussed in §5.

Before discussing these constraints, we can examine the effect of the new reaction rates. The percentage difference in the predicted abundances of d, ^{3}He, ^{4}He, and ^{7}Li was found as each of the reaction rates are individually changed from the CF88 rate to the new rate and as all rates are changed simultaneously. The results for $\eta_{10} = 6.0$ are listed in table 3. The most important change is in the abundance of ^{7}Li at high η values, which is $\approx$ 20 % *lower* with the new rates, substantially affecting the ^{7}Li constraint on η (on Ω_b). From table 3, it is clear that this change is not due to any one particular reaction, but rather to the cumulative effect of changes in all twelve reactions.

5. INFERRED PRIMORDIAL ABUNDANCES

5.1. Introduction

The above sections have described our effort to obtain precise predictions of the d, ^{3}He, ^{4}He, and ^{7}Li abundances with conservative and statistically robust 2-σ uncertainties, as a function of η for 3 neutrino families. In this section, we summarize the observational data on light-element abundances and determine conservative limits on inferred primordial abundances. We must assume that the abundances observed within the solar system (meteoric and solar wind) for deuterium and ^{3}He, within the galaxy (metal-deficient halo stars) for lithium, and extragalactic (nearby H II regions and dwarf galaxies, $\lesssim$ 100 Mpc) for ^{4}He, represent those of the entire universe in order to constrain cosmological parameters.

There are enough observational uncertainties to warrant a very cautious approach in setting abundance limits. Conservative estimates rather than best values are used in order to obtain robust limits on Ω_b and N_ν. A complete discussion of the abundance limits inferred from observations is given in SKM; we will here present details of d + ^{3}He and ^{4}He, which we use to constrain η from below and above, respectively, as well as a brief discussion of ^{7}Li.

5.2. *Primordial d + ^{3}He*

Our ignorance of the details of chemical evolution effects prevents a direct determination of primordial d and ^{3}He. However, the *pre-solar* d abundance can be adopted as a *lower* limit to the primordial deuterium abundance d_p: the pre-solar d abundance should be larger than the present d abundance because of $d(p,\gamma)^3He$ reactions and should not be larger than the primordial value in the absence of any post-Big Bang deuterium production.

The pre-solar abundance of d and ^{3}He can be determined from analysis of the carbonaceous chondrites (CC), which are believed to closely represent the primitive solar system matter out which the sun formed. The gas-rich meteorites (GRM) and solar wind experiments provide data on the present abundance of the two isotopes. If the ^{3}He abundance as determined from the CC samples is adopted as the pre-solar value of ^{3}He, and the ^{3}He as determined from the GRM/solar wind samples is adopted as the combined pre-solar abundance of d *plus* ^{3}He, then the pre-solar d value can be determined as a difference of the two abundances (Black 1971; Geiss and Reeves 1972).

From their study of the available data set compiled in Pagel (1987), Walker *et al.* (1991) arrive at the following 2-σ ranges for the *pre-solar* abundances:

$$1.8 \leq 10^5 y_2 < 3.3 \tag{6a}$$

$$1.3 \leq 10^5 y_3 < 1.8 \tag{6b}$$

$$3.3 \leq 10^5 y_{23} < 4.9\ , \tag{6c}$$

where y represents the number ratio relative to hydrogen and the subscripts 2, 3, and 23 represent the pre-solar d, ^{3}He, and d+^{3}He values, respectively. A lower limit to the primordial d abundance of $d_p \geq 1.8 \times 10^{-5}$ (2-σ) can therefore be adopted.

An upper limit to d_p is more problematic and model dependent; there is no *a priori* determination of the amount of d destruction prior to formation of the pre-solar nebula. Since d is mainly destroyed via $d(p,\gamma)^3He$, some difficulties can be overcome by considering the total sum of d+^{3}He. There still remains, however, the problem of ^{3}He production and destruction in stars. The uncertainty implicit in this process can be conveniently expressed by introducing the 'survival fraction' g_3, which is the fraction of primordial ^{3}He that survives stellar astration. In a simple one-cycle approximation we have

$$y_{23p} \leq y_{23} + (g_3^{-1} - 1) y_3\ , \tag{7}$$

where y_{23p} is the primordial abundance of d+^{3}He. On the assumption that $g_3 \geq 0.25$ (Yang *et al.*; Delbourgo-Salvador *et al.* 1985; Dearborn *et al.* 1986) we have $y_{23p} \leq 9 \times 10^{-5}$. Clearly this number is dependent on the approximations and assumptions of the chemical evolution model adopted (eg. Walker *et al.* 1991), particularly on the initial mass function. Because of the inherent uncertainties of galactic chemical evolution, we are skeptical as to the usefulness of more sophisticated models in this instance; we will therefore adopt the limit of $y_{23p} \leq 9 \times 10^{-5}$ while being aware of its dependence on chemical evolution.

5.3. *Primordial ^{4}He*

^{4}He is very abundant in the universe, making up approximately one quarter of the barvonic mass. Estimates of the ^{4}He abundance can therefore come from a variety of different sources (see Pagel 1987), but it is believed that the most reliable determination comes from the analysis of emission lines in metal-poor extragalactic H II regions and dwarf galaxies where helium is observed via the recombination of He^+. To trace the production of ^{4}He by chemical evolution, the helium mass fraction is plotted as a function of metallicity and linearly-extrapolated to its (assumed) primordial value Y_p at zero metallicity.

The existing H II data useful for determination of Y_p has been recently tabulated by Pagel (1991), who restricts the data set to H II regions with less than 0.25 solar metallicity. Pagel's analysis gives $Y_p = 0.225 \pm 0.005$ (1-σ) with oxygen as the metallicity tracer and $Y_p = 0.229 \pm 0.004$ (1-σ) with nitrogen as the tracer. The question of the most appropriate metallicity tracer has been discussed in Pagel *et al.* (1986); Steigman, Gallacher and Schramm (1989); and Fuller, Boyd and Kalen (1991). Walker *et al.* (1991) have recently re-analyzed a slightly extended version of the data set used in Pagel (1991), arriving at a similar value of Y_p. Further restricting the data set to the 14 lowest-metallicity objects, Fuller *et al.* (1991) determine $Y_p = 0.220 \pm 0.007$ (1-σ) using nitrogen as the tracer, and conclude that $Y_p = 0.22 \pm 0.01$ is a more reasonable assessment of the primordial helium abundance.

Table 4. Observational Constraints

Element	Abundance Limit	Constraint
Deuterium	$d/H \geq 1.8 \times 10^{-5}$	$\eta_{10} \leq 8.52$
Deuterium and Helium-3	$(d + {}^3He)/H \leq 9.0 \times 10^{-5}$	$\eta_{10} \geq 2.86$
Helium-4	$0.21 \leq Y_p \leq 0.24$	$0.63 \leq \eta_{10} \leq 3.77$
Lithium	$1.1 \times 10^{-10} \leq {}^7Li/H \leq 2.3 \times 10^{-10}$ (Pop II)	$1.02 \leq \eta_{10} \leq 5.87$
	${}^7Li/H \leq 1.3 \times 10^{-9}$ (Pop I)	$\eta_{10} \leq 11.3$

We emphasize that the uncertainties on Y_p quoted above are purely statistical; it is not inconceivable that systematic errors may be larger. Possible sources of such errors are collisional excitation, contribution of neutral helium, interstellar reddening, uncertainty of the ionizing UV-flux, and grain depletion. Davidson and Kinman (1985) review these types of error sources and conclude they could contribute as much as ± 0.01 to the uncertainty of Y_p. Pagel (1991) estimates the maximum systematic uncertainty to be somewhat lower, namely ± 0.005 (1-σ). There is the additional possibility that some site in the early galaxy produces significant quantities of ${}^4He$ but very little metals; first generation massive Pop II stars (Bond, Arnett and Carr 1984) are most often discussed in this regard. Such a systematic source of error, implying even lower values of Y_p, would be very difficult to rule out completely.

A quantitative estimate of the systematic errors in a primordial ${}^4He$ abundance determination is difficult to assess. We will adopt $0.21 \leq Y_p \leq 0.24$ as a cautious and reasonable assessment. This range covers the lower limit estimated by Fuller *et al.* (1991) and is bounded by the 2-σ upper limit as determined by Pagel (1991) on the basis of his analysis of the data and his expectation of the systematic errors. The upper limit to Y_p has very important implications: an upper limit of $Y_p < 0.237$, as possibly indicated by the work of Fuller *et al.* (1991), would be inconsistent with the inferred $d + {}^3He$ primordial abundance in the standard model ($N_\nu = 3$). We note that the lower limit on Y_p plays no role in constraining η.

5.4. Primordial Lithium

Of all the primordial isotopes, the problem of inferring from the available data the primordial abundance of ${}^7Li$ remains the most difficult and controversial because of its small abundance [$(Li/H) \sim 10^{-10} - 10^{-9}$] and because of the large spread in the Li abundances observed in stars of different effective temperatures, ages, masses, and compositions.

There are two widely discussed interpretations of the Li abundance data. The first is that the general increase of the upper envelope of the Li abundance data at higher metallicities is attributed to the gradual enrichment of Li in the galaxy from different nucleosynthesis processes. At the low metallicities characteristic of Pop II stars, no significant enrichment or depletion of Li is thought to occur, and the observed uniform plateau of constant Li abundance $[Li] \approx 2.1$ (where $[Li] = 12 + \log(Li/H)$) is thought to closely resemble the pristine primordial abundance. The stellar modeling analysis accounting for small-scale Li depletions in the plateau stars of Deliyannis *et al.* (1990) gives a 2-σ range for the primordial Li abundance of $2.04 \leq [Li]_p \leq 2.21$. When microscopic diffusion (e.g. gravitational settling) effects were included, their result became $2.14 \leq [Li]_p \leq 2.36$. The degree of diffusion is, however, very sensitive to uncertain physics (e.g., opacity.) We will err on the side of caution and adopt the full range of the two estimates as our primordial Li value from Pop II halo stars, $2.04 \leq [Li]_p \leq 2.36$ (2-σ).

The alternative interpretation of the Li abundance data is that significant amounts ($\sim$ Pop I levels, $[Li] \approx 3$) of Li is produced during the Big Bang, and only very small amounts are produced during the history of the galaxy. In this viewpoint, the low Li abundance seen in the Pop II stars is a consequence of depletion mechanisms such as rotational breaking and the subsequent chemical mixing (Pinsonneault *et al.* 1990) in these older stars, and therefore *cannot* be used to place a firm upper limit on the primordial Li. Even though there is a large spread in the Pop I Li abundance, possibly indicative of many depletion mechanisms, the maximum observed Li abundances in these stars seems to be approximately an order of magnitude larger than the Pop II plateau value. There is still a great deal of uncertainty in the input physics for these rotational depletion models, as well as the subsequent galactic chemical evolution of Li.

Spurred by the ever-increasing accumulation of high quality spectra of metal-poor Pop II stars and by new and improved stellar model calculations, an increasing number of researchers have argued for the correctness of the first of the above scenarios. While this is the point of view we will adopt, we will

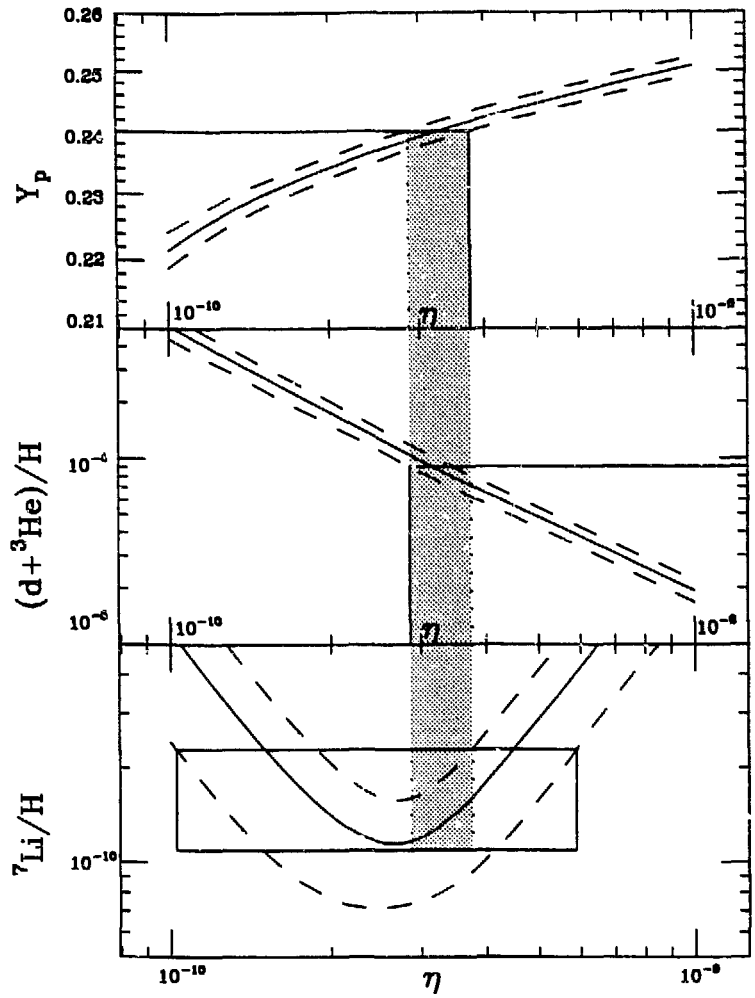

Figure 6. Light-element abundances vs. η for the ^{4}He mass fraction Y_p, (d+^{3}He)/H, and ^{7}Li/H. The boxes indicate observationally acceptable regions for η: the horizontal lines give bounds on the deduced primordial abundances; the vertical lines show the resulting bounds on η. The dashed curves are the 2-σ abundance limits. The shaded regions are the values of η consistent with the observational constraints.

keep in mind that new observations and new models do not allow us to definitively say that the Pop II Li level is the primordial value.

5.5. Summary of Primordial Abundances

Our conservative limits on the primordial abundances inferred from observations are summarized in table 4. The deuterium limit is obtained from the pre-solar value; the d+^{3}He limit from solar system values using a simple one-cycle processing model; the ^{7}Li range from the observations in Pop II metal-deficient stars in the galactic halo; and the ^{4}He range from extrapolations of observations in extragalactic H II regions and dwarf galaxies to zero metallicity. New observations and models do not allow us to definitively say that the Pop II Li level is the primordial value; we have therefore added in table 4 the Pop I level consistent with recent rotational stellar models. We now can compare our model light-element abundance predictions with those inferred from observations.

6. COMPARISON OF OBSERVED AND PREDICTED PRIMORDIAL ABUNDANCES

The uncertainties of our light-element abundance ranges inferred from observations do not have the same statistical significance as the uncertainties on our numerical determinations of the abundance

yields. We can, however, compare the Monte Carlo abundance predictions incorporating the nuclear physics uncertainties to our conservative abundance limits to determine a robust range for η. Such a comparison for the standard BBN model ($N_\nu = 3$) is made in Figure 6, where the abundance limits (the horizontal lines) are shown together with the ^{4}He, d+^{3}He, and ^{7}Li abundance predictions (solid curves) and uncertainties (dashed lines) as functions of η. The observational constraints on η are listed in Table 4. The region of η values consistent with all the observations (the shaded region in Figure 6) is bounded *from below* by the d+^{3}He upper limit, and bounded *from above* by the ^{4}He upper limit:

$$2.86 \leq \eta_{10} \leq 3.77 \; . \tag{8}$$

Our upper bound of 5.87 on η_{10} from ^{7}Li is 47 % higher than the analogous bound found in Walker *et al.* (1991) because the new reaction rates produce $\approx$ 20 % less ^{7}Li at high η values (table 3). Since there is substantially less uncertainty in the primordial ^{4}He abundance than in the primordial ^{7}Li abundance, Y_p gives a *more robust* upper limit on η. Furthermore, since observations of ^{4}He are made over a much larger distance scale than those of ^{7}Li, we have greater confidence in the assumed universality of these limits.

To convert our allowed range of $2.86 \leq \eta_{10} \leq 3.77$ into limits on the present baryon density, we need the present temperature of microwave photons T_γ. The weighted mean of measurements of T_γ at wavelengths $\geq$ 1 mm is $T_\gamma = 2.76 \pm 0.02$ (2–σ), using the results from *COBE* (Mather *et al.* 1990) and from De Amici *et al.* (1991), Gush *et al.* (1990), Kaiser and Wright (1990), Kogut *et al.* (1990), and Meyer *et al.* (1990), as well as the measurements listed in Palazzi *et al.* (1990).

Defining Ω_b as the ratio of baryonic to critical mass density ($\Omega_b = \rho_b/\rho_c$), where $\rho_c = 3H_o^2/8\pi G$ and $H_o = 100h$ km s^{-1} Mpc^{-1} is the Hubble parameter (with uncertainty placed in h), we can express Ω_b as

$$\Omega_b h^2 = 3.73 \times 10^{-3} \left(\frac{T_\gamma}{2.75} \right)^3 \eta_{10} \; . \tag{9}$$

The allowed range of η (eq. 8) can be used along with the above value of T_γ to determine a permitted baryon density range of $0.011 \leq \Omega_b h^2 \leq 0.015$. The factor of $\approx$ 2 uncertainty in the Hubble parameter ($0.4 \leq h \leq 1$; van den Bergh 1989, Visvanathan 1990, Sandage and Tammann 1990) introduces a factor of 4 (by far the largest) in the uncertainty of Ω_b; the SBBN limits are therefore

$$0.01 \leq \Omega_b \leq 0.09 \; . \tag{10}$$

In spite of our cautious approach, our assessment of the constraints on Ω_b may still be disputed. For example, a 3 % increase in the Y_p bound (to 0.247) gives a 55 % increase in the upper limits of η_{10} (to 5.87, equal to that from ^{7}Li) and of Ω_b (to 0.14). The Ω_b lower limit is much less sensitive to changes in the d+^{3}He bound because of the steep η dependence of this sum: increasing this abundance upper bound by 11 % (to 1×10^{-4} as in Walker *et al.*) only results in a 6 % decrease in the η_{10} and Ω_b lower limits. We do believe, however, that our chosen abundance limits, and therefore our Ω_b constraint, are quite robust. Regarding the nuclear physics input, it may be argued that the purely statistical τ_n uncertainty should be used in the Monte Carlo analysis (with no increase for systematic effects); such a change, however, decreases the η upper bound by only 6 %, with the same small effect on the Ω_b upper bound. In our conservative approach, we have chosen to use the larger τ_n uncertainty and slightly larger Ω_b limit.

Several inferences can be drawn from the SBBN constraint in eq. (10). First, the baryon density is more than a factor of 10 less than that required to close the universe ($\Omega = 1$). Second, since the amount of luminous matter in the universe is $\Omega_{lum} \lesssim 0.007$ (e.g. Pagel 1990), baryonic dark matter is *required*. Our SBBN constraint does not, however, guarantee the existence of non-baryonic dark matter (NBDM). The large Ω values determined from galaxy clusters (e.g. $\Omega \approx 0.2$ for the Coma cluster, Hughes 1989), which could be as low as 0.1 with uncertainties, overlap with our Ω_b constraint for *only* the smallest values of the Hubble constant (i.e. $h \approx 0.4$). New studies of distant type-Ia (Sandage *et al.* 1992, Branch 1992) and type-II (Schmidt *et al.* 1992) supernovae suggest, however, that $h = 55 \pm 6$. This H_o limit implies an SBBN limit of $0.03 \leq \Omega_b \leq 0.06$, well below galaxy cluster values, and therefore suggests the existence of NBDM. Alternatively, the SBBN model must be modified to *avoid* NBDM with this H_o limit. Certainly, if even larger values for Ω become well established, such as those tentatively indicated by large scale density fluctuations and peculiar velocities ($\Omega = 0.75 - 1.15$; Yahil 1990, Kaiser *et al.* 1991), then NBDM is unavoidable in SBBN.

We have shown that the SBBN model can *consistently* account for the primordial abundances of d, ^{3}He, ^{4}He, and ^{7}Li inferred from observation within a narrow range of the baryon-to-photon ratio η. There have, however, been efforts to extend the range of Ω_b beyond that allowed for by SBBN (to possibly reach $\Omega_b = 1$) by employing new physics or by relaxing standard model assumptions (reviewed in Malaney and Mathews 1992). In the next section, we investigate slightly non-standard models in which the number of neutrino families is different from 3. Using only the inferred primordial abundances as our barometer, the present study shows that deviations from the SBBN model will be *demanded* if the range of Y_p is determined to be outside the range $0.237 \leq Y_p \leq 0.247$, assuming the constraints on d+^{3}He and ^{7}Li remain firm. An *upper* limit of $Y_p < 0.237$ would conflict with the d+^{3}He limit; although there is tentative evidence suggesting that Y_p lies below 0.237 (Fuller *et al.* 1991), the systematic uncertainties do not yet allow for a strong case. Any deviations from the SBBN model or present abundance limits will most likely come from such changes in Y_p.

New observations of Be and B in very metal-poor halo stars (Ryan *et al.* 1992, Gilmore *et al.* 1991, 1992, and Duncan *et al.* 1992) may also point to the inadequacy of SBBN, since negligible amounts of these nuclides are predicted by the standard model. These may suggest either a new production mechanism such as neutrino nucleosynthesis (Malaney 1992), a modified cosmic ray spallation process (Steigman and Walker 1992, Gilmore *et al.* 1992), or inhomogeneous BBN models (where Ω_b may be significantly enhanced – Boyd and Kajino 1989, Malaney and Fowler 1989). The observations of a Be and B "plateau" in these metal-poor stars would help to differentiate between the proposed scenarios.

Finally, as mentioned in §5.4, a primordial Li abundance at the Pop I level ([Li] $\approx$ 3.1), consistent with the rotational depletion study of Pinsoneault *et al.* (1992), would conflict with the limits from the other light isotopes. More specifically, if a *lower* limit of $[\mathrm{Li}]_p \geq 2.1$ [$(\mathrm{Li/H})_p \geq 1.64 \times 10^{-10}$] can be set for the primordial Li abundance, then there will be a conflict with the limit from ^{4}He ($Y_p < 0.24$).

7. CONSTRAINT ON THE NUMBER OF NEUTRINO FAMILIES

In §6, we compared the predicted abundances (functions of η) for the case of three neutrino families to the abundances inferred from observations; the values of η consistent with observations are within the shaded region in figure 6. Note that a value of N_ν larger than 3 would would increase the ^{4}He abundance for all η values (shift the Y_p curve up in figure 6), since the amount of ^{4}He formed is directly proportional to the number of light (mass $\ll$ 1 MeV) neutrino families. A large enough increase in N_ν would prevent the values of η allowed by the observational constraint $Y_p < 0.24$ from overlapping with η allowed by the constraint $(\mathrm{d} + {}^3\mathrm{He})/\mathrm{H} < 9 \times 10^{-5}$ (i.e. no shaded region in figure 6), and we would conclude that the model was inconsistent with the observations. In efforts to investigate slightly non-standard Big Bang nucleosynthesis models, we have treated N_ν as a variable and searched for the largest value consistent with the observational upper limits.

Our procedure can be described as follows: for a given value of N_ν and a given upper limit on Y_p, we have found the range of upper limits on (d + ^{3}He) which are consistent with observations. This range is shown as a function of the Y_p upper limit in the standard model as the region between the solid lines in figure 7a. Comparison to the single data point in the figure (the observational upper limits for Y_p and (d + ^{3}He)/H) shows that the predictions of the standard model are consistent with the observations. Changing the model to give increased ^{4}He production (e.g., by increasing N_ν from 3.0 to 3.5) changes the range of consistent (d + ^{3}He) upper limits; this shifts the acceptable region in Y_p – (d + ^{3}He) space in figure 7a from between the solid lines to between the dashed lines. Such a change makes the model predictions inconsistent with the observations, and we can therefore rule out 3.5 light neutrino families (three Dirac neutrinos and one Majorana neutrino) at the 2–σ level.

To find the *maximum* allowed value of N_ν, we have duplicated analysis of §4 (1000 Monte Carlo runs at each of 15 η values) for values of N_ν ranging from 2.5 to 5.0. We find that $N_\nu = 3.3$ is the maximum allowed value. This is clear from figure 7b, a plot of the low-abundance (left) edges of the acceptable regions in figure 7a for a variety of N_ν values: for a larger value of N_ν, the allowed region (lying right of the curves) does not overlap with the observations.

Like the upper limit on Ω_b, the N_ν upper limit is very dependent on the observations. A parameterization of this upper limit $(N_\nu)_{upper}$ with respect to the Y_p and d + ^{3}He observational upper limits is given by

$$(N_\nu)_{upper} = 3.30 + 66.1\Delta Y_p + 745(\Delta Y_p)^2 + 5.64\times10^{-3}(\Delta dHe)^{1/2} + 0.625(\Delta dHe) + 0.625(\Delta dHe)^{3/2} \quad (13)$$

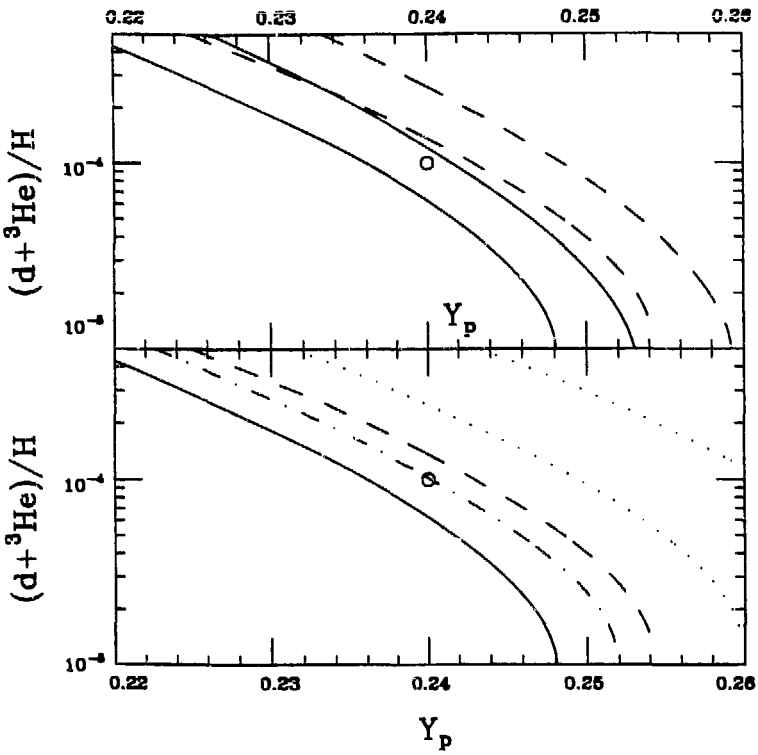

Figure 7. (a) The allowed values of the upper limit of the (d + ^{3}He / H) abundance vs. the upper limit of the ^{4}He mass fraction Y_p, for $N_\nu = 3.0$ (region between solid lines) and 3.5 (region between dashed lines). The data point is the observational upper limits. (b) The lower edge of the allowed regions in (a) for $N_\nu = 3.0$ (solid curve), 3.3 (dotdash), 3.5 (dash), 4.0 (dots), and 5.0 (dots); only for $N_\nu \leq 3.3$ does the allowed region (to the right of the curves) overlap with observations.

where $\Delta Y_p = (Y_p)_{upper} - 0.24$ and $\Delta dHe = (\mathrm{d} + {}^3\mathrm{He} / \mathrm{H})_{upper} \times 10^4$ - 1. This expression is valid for small changes in the Y_p and (d + ^{3}He) upper limits.

8. CONCLUSIONS

We have carried out a comprehensive experimental, computational, and observational analysis of the standard theory of primordial nucleosynthesis, employing a detailed analysis of the rates and uncertainties of the most important nuclear reactions; a Monte Carlo analysis giving robust 2-σ abundance predictions from the reaction rate uncertainties for the primordial isotopes d, ^{3}He, ^{4}He, and ^{7}Li; a correction for errors in abundance predictions which arise from the numerical computation; and the most recent theoretical developments in obtaining inferred primordial abundances from observational data. The comparison of our numerical abundance predictions with those inferred from observations shows that consistent agreement can be achieved for all the light elements over a narrow range of the SBBN parameter η. This range is $2.86 \leq \eta_{10} \leq 3.77$, where the *lower* bound is from the primordial d + ^{3}He abundance and the *upper* bound is from the primordial ^{4}He abundance; this is in contrast to previous studies which used the less certain primordial ^{7}Li abundance to bound η from above. The permitted range of η corresponds to a constraint on the baryon mass density parameter of $0.01 \leq \Omega_b \leq 0.09$. In determining this conservative constraint on Ω_b, we have assumed 3 relativistic neutrino species and the universality of the abundance observations used to infer primordial abundances. An investigation of slightly non-standard BBN models representing cosmologies with 2.5 to 5 neutrino families shows that $N_\nu \leq 3.3$ is required for consistency with the observational upper limits on ^{4}He and d + ^{3}He.

Additional observational work is necessary to further constrain Ω_b, since the largest remaining uncertainties are from the Hubble parameter H_o and the primordial abundances inferred from observational data. From the nuclear laboratories, high-precision measurements of d(p, γ)^{3}He, d(d, n)^{3}He, d(d, p)t, t(α, γ)^{7}Li up to energies of 1 MeV would be quite useful.

The exciting possibility exists, however, that modifications to the SBBN model will be necessary; this would be the case in light of a further lowering of the primordial ^{4}He abundance (to below 0.237) or of the observation of a plateau in the Be and B abundances in extremely metal-poor stars. It will be of wide-ranging interest, particularly with regard to non-baryonic dark matter or inhomogeneous models, to observe if the validity and consistency of SBBN theory remains intact.

Acknowledgments

I would like to acknowledge my collaborators on this work, Lawrence H. Kawano and Robert A. Malaney, and would additionally like to thank Dick Azuma, Charles Barnes, Timothy Beers, Richard Boyd, Carl Brune, Michel Casse, Constantine Deliyannis, Willy Fowler, Ralph Kavanagh, Lawrence Krauss, Peter Parker, Erich Ormand, Kenneth Sale, and Wallace Sargent for helpful discussions. This work was supported at Caltech by the NSF under grants PHY88-17296 and PHY91-15574, by the Oak Ridge National Laboratory Postdoctoral Research Program administered by the Oak Ridge Institute for Science and Education, and by the Department of Energy contract DE-AC05-84OR21400 with Martin Marietta Energy Systems, Inc.

References

Alfimenkov, V. P., *et al.*, 1980, JINR, R3-80-394, Dubna.
Altmeyer, T., Kolbe, E., Warmann, T., Langanke, K., & Assenbaum, H. J., 1988, *Z. Phys.*, **A330**, 277.
Arnold, W. R., Phillips, J. A., Sawyer, G. A., Stovall, E. J. Jr., & Tuck, J. L., 1954, *Phys. Rev.*, **93**, 483.
Baur, G., Bertulani, C. A., & Rebel, H., 1986, *Nucl. Phys.*, **A458**, 188.
Beaudet, G., & Reeves, H., 1984, *Astr. Ap.*, **134**, 240.
Bethe, H. A., & Morrison, P., 1956, *Elementary Nuclear Theory*, (New York: Wiley), 2nd ed., p. 75.
Black, D. C., 1971, *Nature Phys. Sci*, **231**, 1480.
Bond, J. R., Arnett, W. D. & Carr, B., 1984, *Ap. J.*, **280**, 825.
Bondarenko, L. N., Kurguzov, V. V., Prokof'ev, Yu. A., Rogov, E. V., & Spivak, P. E., 1978, *JETP Lett.*, **28**, 303.
Booth, D. L., Preston, G. R., & Shaw, P. F. D., 1956, *Proc. Phys. Soc. London*, **A69**, 265.
Bosman, M., Bol, A., Gilot, J. F., Leleux, P., Lipnik, P., & Macq, P., 1979, *Phys. Lett.*, **82B**, 212.
Boyd, R. N., & Kajino, T., 1989, *Ap. J. Lett.*, **336**, L55.
Branch, D., 1992, *Ap. J.*, **392**, 35.
Brown, R. E., & Jarmie, N., 1990, *Phys. Rev.*, **C41**, 1391.
Brune, C., Kavanagh, R. W., & Rolfs, C. R., 1991, private communication.
Burzynski, S., Czerski, K., Marcinkowski, A., & Zupranski, P., 1987, *Nucl. Phys.*, **A473**, 179.
Byrne, J., 1982, *Rep. Prog. Phys.*, **45**, 115.
Caughlan, G. R., & Fowler, W. A., 1988, *Atomic Data & Nucl. Data Tables*, **40**, 291.
Clayton, D. D., 1983, *Principles of Stellar Evolution & Nucleosynthesis*, (Chicago: Univ. of Chicago Press).
D'Antona, F. & Mazzitelli, I., 1984, *Astr. Ap.*, **138**, 431.
Davidson, K. & Kinman, T. D., 1985, *Ap. J. Supp.*, **58**, 321.
De Amici, G., Bersanelli, M., Kogut, A., Levin, S., Limon, M., & Smoot, G. F., 1991, *Ap. J.*, **381**, 341.
Dearborn, D. S. P. , Schramm, D. N. & Steigman, G., 1986, *Ap. J.*, **302**, 35.
Delbourgo-Salvador, P., Gry, C., Malinie, G., & Audouze, J., 1985, *Astr. Ap.*, **150**, 53.
Deliyannis, C. P., Demarque, P., & Kawaler, S. D., 1990, *Ap. J. Supp.*, **73**, 21.
Deliyannis, C. P. & Pinsonneault, M. H., 1993, *Ap. J.*, submitted.
Dicus, D. A., Kolb, E. W., Gleeson, A. M., Sudarshan, E. C. G., Teplitz, V. L., & Turner, M. S., 1982, *Phys. Rev.*, **D26**, 2694.
Dubbers, D., 1991, *Prog. Part. Nucl. Phys.*, **26**, 173.
Duncan, D., Lambert, D., & Lemke, D., 1992, *Ap. J.*, **401**, 584.
Evans, R. D., 1955, *The Atomic Nucleus*, (New York: McGraw Hill).
Fowler, W. A., Caughlan, G. R., & Zimmerman, B. A., 1967, *Ann. Rev. Astr. Ap.*, **5**, 525.
Fowler, W. A., Caughlan, G. R., & Zimmerman, B. A., 1975, *Ann. Rev. Astr. Ap.*, **13**, 69.
Freedman, S., 1990, *Comm. Nucl. Part. Phys.*, **19**, 209.
Fuller, G. M., Boyd, R. N., & Kalen, J. D., 1991, *Ap. J. Lett.*, **371**, L11.
Ganeev, A. S., Govorov, A. M., Osetinskii, G. M., Rakivnenko, A. N., Sizov, I. V., & Siksin, V. S., 1957, *Atomnaya Energiya Supp.*, **5**, 21.
Geiss, J. & Reeves, H., 1972, *Astr. Ap.*, **18**, 126.
Gilmore, G., Edvardson, B., & Nissen, P., 1991, *Ap. J.*, **378**, 17.
Gilmore, G., Gustafson, B., Edvardson, B., & Nissen, P. E., 1992, *Nature*, **357**, 379.
Griffiths, G. M., Morrow, R. A., Riley, P. J., & Warren, J. B., 1961, *Can. J. Phys.*, **39**, 1397.
Gush, H. P., Halpern, M., & Wishnow, E. H., 1990, *Phys. Rev. Lett.*, **65**, 537.
Hale, G. M., Dodder, D. C., Siciliano, E. R., & Wilson, W. B., 1991, ENDF/B-VI Evaluation, Material 125, Revision 1.

Harris, M. J., Fowler, W. A., Caughlan, G. R., & Zimmerman, B. A., 1983, Ann. Rev. *Astr. Ap.*, **21**, 165.
Hikasa, K., *et al.*, 1992, *Phys. Rev.*, **D45**, S1.
Hill, J. C., Wohn, F. K., Schwellenbach, D. D., & Smith, A. R., 1991, *Phys. Lett.*, **B273**, 371.
Horsley, A.,1966, *Nuc. Data*, **A2**, 243.
Hughes, D. J., & Schwartz, R. B., 1958, Brookhaven Natl. Lab. Rept. BNL 325, 2nd ed.
Hughes, J. P., 1989, *Ap. J.*, **337**, 21.
Howerton, R. J., 1959, Univ. California Radiation Lab. Rep. No. 5226 (Berkeley, CA: Univ. of California).
Kaiser, M. E., & Wright, E. L., 1990, *IAU Symp.*, **139**, 390.
Kajino, T., 1986, *Nucl. Phys.*, **A460**, 559.
Kajino, T., & Arima, A., 1984, *Phys. Rev. Lett.*, **52**, 739.
Kajino, T., Toki, H., & Austin, S. M., 1987, *Ap. J.*, **319**, 531.
Kajino, T., Mathews, G. J., & Ikeda, K., 1989, *Phys. Rev.*, **C40**, 525.
Kawano, L. H., 1988, FERMILAB-PUB-88/34-A, preprint.
Kawano, L. H., 1992, Caltech Kellogg Radiation Lab OAP-714, preprint; FERMILAB-PUB-92/04-A, preprint.
Kogut, A., Bensadoun, M., De Amici, G., Levin, S., Smoot, G. F., & Witebsky, C., 1990, *Ap. J.*, **355**, 102.
Krauss, A., Becker, H. W., Trautvetter, H. P., Rolfs, C., & Brand, K., 1987, *Nucl. Phys.*, **A465**, 150.
Krauss, L. M., & Romanelli, P., 1990, *Ap. J.*, **358**, 47.
Langanke, K., 1986, *Nucl. Phys.*, **A457**, 351.
Last, J., Arnold, J., Dohner, J., Dubbers, D., & Freedman, S.J., 1988, *Phys. Rev. Lett.*, **60**, 995.
Malaney, R. A., 1992, *Ap. J. Lett.*, **398**, L45.
Malaney, R. A., & Fowler, W. A., 1989, *Ap. J. Lett.*, **345**, L5.
Malaney, R. A., & Mathews, G. J., 1992, *Phys. Reports*, in press.
Mampe, W., Ageron, P., Bates, C., Pendlebury, J. M., & Steyerl, A., 1989, *Nucl. Inst. Meth.*, **A284**, 111; 1989, *Phys. Rev. Lett.*, **63**, 593.
Mason, J. E., Gazes, S. B., Roberts, R. B., & Teichmann, S. G., 1992, Univ. Rochester Nucl. Struct. Lab NSRL-378, preprint.
Mather, J. C., *et al.*, 1990, *Ap. J. Lett.*, **354**, L37.
McNeill, K. G., & Keyser, G. M., 1951, *Phys. Rev.*, **81**, 602.
Mertelmeier, T., & Hofmann, H. M.,1986, *Nucl. Phys.*, **A459**, 387.
Meyer, D. M., Roth, K. C., & Hawkins, I., 1990, *IAU Symp.*, **139**, 392.
Mughabghab, S. F., Divadeenam, M., & Holden, N.E., 1981, *Neutron Cross Sections, Vol. 1, Neutron Resonance Parameters & Thermal Cross Sections, Part A, Z=1-60*, (New York: Academic Press).
Pagel, B. E. J., 1986, in *Inner Space/Outer Space*, ed. E.W. Kolb, M. S. Turner, D. Lindley, K. Olive & D. Seckel (Chicago: Univ. of Chicago Press), p. 72.
Pagel, B. E. J., Terlevich, R. J. & Melnick, J. 1986, *P. A. S. P.*, **98**, 1005.
Pagel, B. E. J., 1987, in *A Unified View of the Macro & Micro Cosmos*, ed. A. De Rujula, D. V. Nanopoulos, & P. A. Shaver, (World Scientific: Singapore), p. 399.
Pagel, B. E. J., 1990b, in *Baryonic Dark Matter*, ed. D. Lynden-Bell & G. Gilmore (Kluwer: Netherlands) p. 237.
Pagel, B. E. J., 1991, *Phys. Scripta*, **T36**, 7.
Palazzi, E., Mandolesi, N., Crane, P., Kutner, M. L., Blades, J. C., & Hegyi, D. J., 1990, *Ap. J.*, **357**, 14.
Pinsonneault, M. H., Kawaler, S. D., & Demarque, P., 1990, *Ap. J. Supp.* , **74**, 501.
Pinsonneault, M. H., Deliyannis, C. P. & Demarque, P., 1992, *Ap. J. Supp.* , **78**, 179.
Preston, G., Shaw, P. F. D., & Young, S. A., 1954, *Proc. Roy. Soc.*, **A226**, 206.
Riley, S. P., & Irvine, J. M., 1991, *J. Phys.*, **G17**, 35.
Rolfs, C., & Rodney, W. S., 1988, *Cauldrons in the Cosmos*, (Chicago: Univ. of Chicago).
Ryan, S., *et al.*, 1992, *Ap. J.*, **388**, 184.
Sandage, A., & Tammann, G. A., 1990, *Ap. J.*, **365**, 1.
Sandage, A., Saha, A., Tammann, G., Panagia, N., & Macchetto, F., 1992, *Ap. J. Lett.*, **401**, L7.
Schmidt, B., Kirshner, R., & Eastman, R., 1992, *Ap. J.*, **395**, 366.
Schroder, U., Redder, A., Rolfs, C., Azuma, R. E., Buchmann, L., Campbell, C., King, J. D., & Donoghue, T. R., 1987, *Phys. Lett.*, **142B**, 55.
Shapiro, F. L., 1958, *Sov. Phys. JETP*, **7**, 1132.
Spite, M. & Spite, F., 1982, *Astr. Ap.*, **115**, 357.
Spivak, P. E., 1966, *Sov. Phys. JETP*, **67**, 1735.
Steigman, G., 1990, in *Primordial Nucleosynthesis*, eds. W. J. Thompson, B. W. Carny, H. J. Karwowski (World Scientific: Singapore) p. 1.
Steigman, G., Gallagher, J. & Schramm, D. N., 1989, *Comm. Astrophys.*, **14**, 97.
Steigman, G., & Walker, T. P., 1992, *Ap. J.*, **385**, L13.
Utsunomiya, H., *et al.*, 1990, *Phys. Rev. Lett.*, **65**, 847.
van den Bergh, S., 1989, *Astron. Astrophys. Rev.*, **1**, 111.
Visvanathan, N., 1990, *Aust. J. Phys.*, **43**, 189.
Wagoner, R. V., 1969, *Ap. J. Suppl.*, No. 162, **18**, 247.
Walker, T. P., Steigman, G., Schramm, D. N., Olive, K. A., & Kang, H.-S., 1991, *Ap. J.*, **376**, 51.
Yahil, A., 1990, in *Particle Astrophysics*, ed. J.-M. Alimi, A. Blanchard, A. Bouquet, F. M. de Volnay, J. T. T. Van (Editions Frontiers: France) p. 483.
Yang, J., Turner, M. S., Steigman, G., Schramm, D. N., & Olive, K. A., 1984, *Ap. J.*, **281**, 493.

DISCLAIMER